Quantitative SAXS Analysis of Oriented 2D Hexagonal Cylindrical Silica Mesostructures in Thin Films Obtained from Nonionic Surfactants

Bernd Smarsly,*,[†,‡] Alain Gibaud,[§] Wilhelm Ruland,[∥] Dietmar Sturmayr,[⊥] and C. Jeffrey Brinker[‡,⊥]

Max-Planck Institute of Colloids and Interfaces, Am Mühlenberg 1, D-14476 Potsdam-Golm, Germany, University of New Mexico, Advanced Materials Lab, 1001 University Boulevard, Albuquerque, New Mexico 87106, Laboratoire de Physique de l'Etat Condensé, UMR CNRS 6087, Université du Maine, 72085 Le Mans Cedex 09, France, University of Marburg, Fachbereich Chemie, D-35032 Marburg, Germany, and Sandia National Laboratories, MS 1349, Albuquerque, New Mexico 87185

Oriented mesostructured surfactant–silica nanocomposite thin films with a 2D hexagonal mesostructure of cylindrical micelles were prepared by evaporation-induced self-assembly using two different nonionic Brij surfactants and studied by small-angle X-ray scattering in symmetric reflection (SRSAXS) and grazing incidence (GISAXS) geometries. A novel SRSAXS evaluation approach was applied that allowed a good fitting of the SRSAXS data over almost the whole range of scattering vectors. Aside from the cylinder radius and the lattice parameter, the approach provided accurate values for the polydispersity of the micelles, lattice distortions, and preferred orientation. These analyses revealed a significant rise of the micelle radius and accordingly the lattice parameter upon an increase in the ratio surfactant/SiO₂, attributable to a decrease in the solubilization of the poly(ethylene oxide) (PEO) chains by water, in agreement with Monte Carlo simulations. Furthermore, the SRSAXS analysis was successfully applied to the corresponding mesoporous films for the determination of pore sizes.

Introduction

The preparation of surfactant-templated silica thin films, possessing various types of nanoscopic mesostructures such as 2D hexagonal cylinders or 3D hexagonal and cubic lattices, has attained great attention, because they are believed to show high promise for various applications. As the key step, sol–gel chemistry is combined with surfactant-mediated evaporation-induced self-assembly (EISA).[1a] Typically, a substrate is dip-coated or spin-coated with an acidic aqueous solution of a structure-directing surfactant such as cetyltrimethylammonium bromide (CTAB) or block copolymers such as "Brij" type surfactants or P123, a silica precursor such as tetraethyl orthosilicate (TEOS) and a water-miscible, volatile solvent (e.g., ethanol). Upon solvent evaporation, at a certain concentration co-self-assembly of the surfactant and the silica precursors leads to mesostructures such as lamellae and cylindrical rods. The characterization of thin mesostructured films (having a thickness of only

several hundred nanometers) is more difficult in comparison with corresponding bulk materials due to the low quantities. Recently, based on in situ grazing incidence small-angle X-ray scattering (GISAXS), in particular by time-resolved GISAXS experiments,[1,2] significant progress was reported in various publications (Grosso et al., Gibaud et al., and Brinker's group) that have provided a thorough characterization and a profound understanding of the parameters determining the mesostructure formation. GISAXS turned out to be an invaluable tool for the exact characterization of the type of mesostructure. For instance, these studies have addressed the influence of various parameters on the mesostructure, such as the evaporation rate and the external humidity.[2h] Aside from the type of the mesostructure, the determination of the exact structural parameters is crucial for a thorough characterization of mesostructured films. In particular, it is desirable to obtain accurate values for the mesopore (or micellar) size and the wall thickness. However, these parameters were almost inaccessible so far due to the lack of suitable

* Corresponding author. E-mail: smarsly@mpikg.mpg.de.
† Max-Planck Institute of Colloids and Interfaces.
‡ University of New Mexico.
§ Université du Maine.
∥ University of Marburg.
⊥ Sandia National Laboratories.

(1) (a) Brinker, C. J.; Lu, Y. F.; Sellinger, A.; Fan H. Y. *Adv. Mater.* **1999**, *11*, 579–585. (b) Gibaud, A.; Grosso, D.; Smarsly, B.; Baptiste, A.; Bardeau, J. F.; Babonneau, F.; Doshi, D. A.; Chen, Z.; Brinker, C. J.; Sanchez, C. *J. Phys. Chem. B* **2003**, *107*, 6114–6118. (c) Doshi, D. A.; Gibaud, A.; Goletto, V.; Lu, M. C.; Gerung, H.; Ocko, B.; Han, S. M.; Brinker, C. J. *J. Am. Chem. Soc.* **2003**, *125*, 11646. (d) Doshi, D. A.; Gibaud A.; Liu, N. G.; Sturmayr, D.; Malanoski, A. P.; Dunphy, D. R.; Chen, H. J.; Narayanan, S.; MacPhee, A.; Wang, J.; Reed, S. T.; Hurd, A. J.; van Swol, F.; Brinker, C. J. *J. Phys. Chem. B* **2003**, *107*, 7683. (e) Miyata, H.; Noma, T.; Watanabe, M.; Kuroda, K. *Chem. Mater.* **2002**, *14*, 766. Alberius, P. C. A.; Frindell, K. L.; Hayward, R. C.; Kramer, E. J.; Stucky, G. D.; Chmelka, B. F. *Chem. Mater.* **2002**, *14*, 3284–3294.

(2) (a) Grosso, D.; Balkenende, A. R.; Albouy, P. A.; Ayral, A.; Amenitsch, H.; Babonneau, F. *Chem. Mater.* **2001**, *13*, 1848–1856. (b) Grosso, D.; Babonneau, F.; Soler-Illia, G. J. A. A.; Albouy, P. A.; Amenitsch, H. *Chem. Commun.* **2002**, 748–749. (c) Klotz, M.; Albouy, P. A.; Ayral, A.; Ménager, C.; Grosso, D.; Van der Lee, A.; Cabuil, V.; Guizard, C. *Chem. Mater.* **2000**, *12*, 1721–1728. (d) Gibaud, A.; Grosso, D.; Smarsly, B.; Baptiste, A.; Bardeau, J. F.; Babonneau, F.; Doshi, D. A.; Chen, Z.; Brinker, C. J.; Sanchez, C. *J. Phys. Chem. B* **2003**, *107*, 6114–6118. (e) Grosso, D.; Balkenende, A. R.; Albouy, P. A.; Lavergne, M.; Babonneau, F. *J. Mater. Chem.* **2000**, *10*, 2085–2089. (f) Grosso, D.; Babonneau, F.; Albouy, P. A.; Amenitsch, H.; Balkenende, A. R.; Brunet-Bruneau, A.; Rivory, J. *Chem. Mater.* **2002**, *14*, 931–939. (g) Besson, S.; Gacoin, T.; Jacquiot, C.; Ricolleau, C.; Babonneau, F.; Boilot, J.-P. *J. Mater. Chem.* **2000**, *10*, 1331–1337. (h) Cagnol, F.; Grosso, D.; Soler-Illia, G. J. D. A. S.; Crepaldi, E. L.; Babonneau, F.; Amenitsch, H.; Sanchez, C. *J. Mater. Chem.* **2003**, *13*, 61–66. (i) Smarsly, B.; Grosso, D.; Brezesinski, T.; Pinna, N.; Boissiere, C.; Antonietti, M.; Sanchez, C. *Chem. Mater.* **2004**, *16*, 2948–2952.
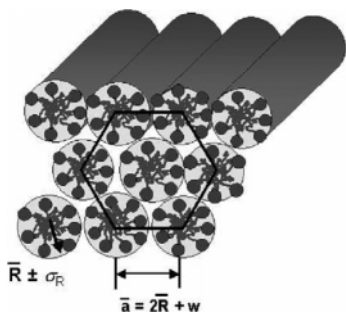
Figure 1. Schematics of a 2D hexagonal arrangement of micellar cylinders, showing the main geometric parameters. The wall thickness can be defined via the average cylinder radius $\bar{R}$ and the average lattice parameter $\bar{a}$. The illustration indicates a slight deviation from a uniform geometry in terms of lattice distortions and a distribution of cylinder radii.

experimental techniques. Physisorption techniques have been specially developed for thin films and successfully applied to porous coatings ("surface acoustic wave" technique developed by Brinker et al.[3]) but suffer from practical shortcomings. Also, positron annihilation lifetime spectroscopy (PALS) does not represent an analytical technique for a routine determination of porosity in thin mesostructured films.[4,5] Moreover, these techniques are not applicable for nonporous nanocomposite organic–inorganic mesostructured films.

In the present study SAXS in symmetric reflection (abbreviated as SRSAXS, in analogy to GISAXS) was applied to determine the structural parameters of silica mesostructured thin films obtained from nonionic Brij surfactants (n-alkyl-poly(ethylene oxide), "C_xE_y" type surfactants). Two surfactants were used, differing in the length of the hydrophobic tail ("Brij 58" with $x = 16$ and $y = 20$ and "Brij 56" with $x = 10$ and $y = 20$). The formulation used resulted in highly regular 2D hexagonal mesostructures of cylindrical micelles, with the cylinders being oriented parallel to the substrate (Si wafer or glass). In a previous publication on CTAB-based silica nanocomposite films showing a 2D hexagonal morphology, it was already proven that this technique provides invaluable information on the mesostructure.[6] It was demonstrated that X-ray scattering in reflection geometry, obtained from highly regular mesostructures, shows pronounced interference maxima and minima, originating from the lattice and form factor, respectively. As a general idea, it was proposed to fit SRSAXS data by a suitable structural model, within the Born approximation, with a limited number of physically meaningful structural parameters, in particular the average micelle radius $\bar{R}$ and an average lattice parameter $\bar{a}$ (see Figure 1). A similar treatment was developed for lamellar mesostructured films.[8] Usually, in most of the publications on similar materials, the analysis of such SAXS data does not go beyond the determination of the long period from the position of interferences ("Bragg peaks"). The present study has to be regarded as an extension of the previous concept in ref 6 in terms of a more detailed analysis of SAXS data. We want to emphasize that the X-ray investigation was

referred to as "X-ray reflectivity" in the previous publication.[6] However, we prefer to use the terminology "SAXS in symmetric reflection" (SRSAXS) in order to point out that we use the kinematic approximation applied to thin films, which basically has to be regarded as "classical" SAXS on oriented mesostructures.

The objective of the present study is manifold: First, a recently introduced general evaluation,[7] developed as an extension of the concept shown in ref 6, is applied to the SRSAXS of different films obtained from two surfactants, to check the validity of this extended approach. In ref 7, it had been demonstrated that several structural parameters (see below) of 2D hexagonal arrays of oriented cylinders can be extracted with high precision and accuracy on the angstrom scale from experimental SRSAXS data. Simulations were carried out to illustrate the influence of various structural parameters on the SRSAXS curves. As an important extension, in the present study, mesoporous films obtained by calcination of the hybrid films were studied in order to determine the pore size and wall thickness.

Second, a series of SRSAXS experiments was performed on various Brij-based mesostructured films, prepared from solutions of the two surfactants with different surfactant concentrations. A concentration regime was chosen, where in all cases a 2D hexagonal mesostructure was observed. Thereby, it was possible to assess the influence of the surfactant/silica ratio on the micelle size and the wall thickness by the extended SRSAXS analysis. Since the changes in these parameters are small, no comparable study has been performed so far due to the lack of appropriate characterization techniques. Recently, Antonietti et al. had reported that for nonionic block copolymers an increase in the template concentration resulted in an increase in the mesopore size in bulk silica.[9] In addition, our high-precision SAXS analyses were expected to shed more light onto the distribution of the EO units, which were reported to penetrate the silica walls.[10] Our study therefore aims at gaining greater insights into the self-assembly of poly(ethylene oxide) (PEO)-containing block copolymers in thin films.

Third, the dependence of the cylinder radius on the surfactant concentration was interpreted in terms of suitable theoretical concepts. Aside from a qualitative interpretation based on the concept of the packing parameter, Monte Carlo simulations were performed on suitable model systems and compared with the results obtained from SRSAXS. In conclusion, this study is dedicated to a better understanding of the influence of the composition of templating solutions on the mesostructure of the final nanocomposite thin films.

Experimental Section

The GISAXS experiments were carried out at the 1 BM C beamline (10 keV) at Argonne National Labs (APS). The data were collected by a CCD camera (1024×1024 pixels). SRSAXS measurements were performed at the 1 BM C beamline at APS and the X22A beamline at Brookhaven National Labs, the latter working at a fixed energy of 11 keV. The measurements were carried out under strictly specular conditions. For both setups, the experimental and electronic background scattering turned out to be about 3 orders of magnitude lower than the signals from the samples. For SRSAXS and reflectivity experiments, a refraction correction must be applied if the intensity is measured close to the critical angle of external reflection of the substrate.

(3) Frye, G. C.; Ricco, A. J.; Martin, S. J.; Brinker, C. J. *Mater. Res. Soc. Symp. Proc.* **1988**, *121*, 349.

(4) Gregory, R. B. *J. Appl. Phys.* **1991**, *70*, 4665.

(5) Dlubek, G.; Hubner, C. and Eichler, S. *Nucl. Instrum. Methods Phys. Res., Sect. B* **1998**, *142*, 191.

(6) Gibaud, G.; Baptiste, A.; Doshi, D. A.; Brinker, C. J.; Yang, L.; Ocko, B. *Europhys. Lett.* **2003**, *63*, 833–839.

(7) Ruland, W.; Smarsly, B. *J. Appl. Crystallogr.* **2005**, *38*, 78–86.

(8) Ruland, W.; Smarsly, B. *J. Appl. Crystallogr.* **2004**, *37*, 575–684.

(9) Thomas, A.; Schlaad, H.; Smarsly, B.; Antonietti, M. *Langmuir* **2003**, *19*, 4455.

(10) Göltner, G.; Smarsly, B.; Berton, B.; Antonietti, M. **2001**, *13*, 1617–1624.

Table 1. Structural Parameters for the Brij 58− and Brij 56−Silica Hybrid Films Obtained from the Reflectivity Analysis Based on eq 2[a]

		radius $\bar{R}$ from fit (Å)	radius R_1 from minimum s_1 (Å)	σ_R (Å)	lattice constant $\bar{a}$ (Å)	σ_a (Å)	interfacial width d_z (Å)	wall thickness w (Å)
Brij 58−silica	sample 1,	30.2	31.3	0.5	65.1	2.1	4.0	8.7
	$c/c_0 = 0.9$	(12.5)		(0.9)	(36.8)	(1.0)	(5.3)	(17.1)
	sample 2,	32.0	34.1	0.2	67.5	2.1	4.2	7.7
	$c/c_0 = 1.0$	(14.0)		(0.9)	(37.8)	(1.0)	(4.3)	(14.1)
	sample 3,	33.1	35.3	0.4	69.8	1.8	4.2	7.9
	$c/c_0 = 1.1$	(15.1)		(1.2)	(39.2)	(1.4)	(5.2)	(14.2)
Brij 56−silica	sample 4	27.6	29.4	0.4	58.2	1.5	4.1	7.2
	$c/c_0 = 0.9$	(12.0)		(0.8)	(34.5)	(1.1)	(4.2)	(14.7)
	sample 5	29.8	31.2	0.3	63.2	1.9	3.9	7.5
	$c/c_0 = 1.0$	(13.3)		(0.9)	(35.8)	(1.3)	(4.2)	(13.4)
	sample 6	30.6	32.0	0.4	65.0	1.6	4.0	7.8
	$c/c_0 = 1.1$	(14.2)		(0.9)	(37.3)	(1.1)	(4.0)	(12.9)

[a] The values in parentheses were obtained from the calcined silica films. R_1 was determined using eq 4. The wall thickness was determined using eq 3. The parameter B_{ax} (a measure for the preferred orientation, see ref 7) was only determined for samples 1−3 and was ∼0.03 ± 0.01° for all three samples. The parameters for sample 1 correspond to those presented already in ref 7.

To take into account the refraction correction, the modulus of the scattering vector $s = 2/\lambda \sin\theta$ must be replaced by the corrected value $s = \sqrt{s_{obs}^2 - s_c^2}$, where s_c corresponds to the critical wave vector of Si and s_{obs} to the experimental value. However, as soon as the scattering vector becomes larger than the critical wave vector of silicon, this effect is negligible. This is the case in the following data analysis. The half of the width of the slit function $W(y)$ was $y_{max} = 0.2$ nm^{-1}.

The transmission electron microscopy (TEM) study was performed on material scratched off the film, using a JEOL 2010 instrument operated at 200 kV. The TEM images were acquired with a Gatan slow scan CCD camera.

The silica−organic nanocomposite mesostructured films were prepared by a single dip-coating step (20 cm/min) on a Si wafer (finally leading to a film surface of 1 cm × 4 cm) with a stock solution ("A2**") containing a silica precursor (tetraethyl ortho-silicate, TEOS), ethanol, hydrochloric acid, and the Brij surfac-tants. The films were treated at 80 °C for 1 h to remove the solvent. Brij surfactants are low-molecular-weight amphiphilic (alkyl-poly(ethylene oxide) block copolymers of the type C_xE_y with $x = 16$ and $y = 20$ for Brij 58 and $x = 10$ and $y = 20$ for Brij 56. Details for the preparation of A2** are given in ref 6. The solutions to be dip-coated were prepared by dissolving m grams of the surfactant in 10 mL of A2**, 20 mL of EtOH, and 1.6 g of hydrochloric acid (1 M), using an external humidity of 30% RH. Various concentrations of the surfactant were studied; in this publication, we present three examples, referred to in the following as "sample 1" (Brij 58, $m = 1.1$ g, $c/c_0 = 0.9$), "sample 2" (Brij 58, $m = 1.25$ g, used as the reference solution $c/c_0 = 1$), and "sample 3" (Brij 58, $m = 1.3$ g, $c/c_0 = 1.1$). The corresponding samples for the Brij 56 are called "samples 4−6" (see Table 1), using identical amounts of the corresponding ingredients as for the system Brij 58−silica. Both surfactants showed a comparable behavior with respect to the occurrence of the 2D hexagonal phase. The film thicknesses were determined by spectroscopic ellip-sometry; we obtained 280 nm (sample 1), 300 nm (sample 2), and 320 nm (sample 3) and similar values for samples 4−6. To obtain porous films, they were heat-treated in an oven of $T = 450$ °C for 3 h in air, applying a heating ramp of 3 °C/min.

The porous silica samples, used for studying the influence of the hydration of PEO on the porosity, were obtained by a procedure described recently.[16c] The synthesis of the porous silicas was carried out by dissolving PEO in TEOS under moderate heating. Hydrochloric acid (1 M) was added at room temperature,

which causes exothermal hydrolysis of TEOS. To remove the ethanol, the mixture was evacuated on a rotary evaporator at 50 °C for 10 min. Finally, the samples were heat-treated at 450 °C to remove the polymer. The molar ratio PEO/(added water) was varied between 0 and 4.

The nitrogen sorption measurements at 77 K were performed on an ASAP 2000 instrument (Quantachrom).

SAXS Analysis

1. SAXS in Symmetric Reflection of Arrays of Cylinders with a Finite Distribution of Radii, Substitutional Disorder, and a Finite Preferred Orientation. In the following, the SAXS of cylindrical mesostructures, measured in symmetric reflection, is briefly reviewed, summarizing our recently published approach.[7] Real mesostructured materials may contain a small but measurable variance σ_R in the cylinder radius R leading to a smoothing of the interference minima. For highly regular mesostructures, the effect of a variation in size (polydispersity) on SRSAXS data is similar to the effect of variation in shape. In ref 7, a general expression was introduced assuming a radius number distribution of the radius $h(R)$ with variance σ_R and an average radius $\bar{R}$. Furthermore, this approach takes into account a lattice factor $|Z_{h0}|^2(s)/N$, including translational disorder in the direction perpendicular to the substrate (with average distance $\bar{d}_{10}$ and variance σ_{10}) and a finite number $\bar{N}$ (with variance σ_N) of stacks of layers of cylinders, with both effects leading to a broadening of the interference maxima. Within this assumption, we consider the distribution of d_{10} to represent a 1D point lattice with a long period $\bar{d}_{10} = \bar{a}\sqrt{3}/2$.[7] As a main result of the treatment given in ref 7, the lattice factor $|Z_{h0}|^2(s)/N$ and the Laue scattering $\langle|\Phi_R|^2\rangle - |\langle\Phi_R\rangle|^2$ due to the polydispersity of R ($\Phi_R = (R/s)J_1(2\pi Rs)$, $\langle\,\rangle$ stands for average over R) are affected differently by a finite preferred orientation of the meso-structure relative to the substrate. Taking also into account slit smearing from the experimental setup, the theoretical SRSAXS $J_{sr}(s)$ of such nanocomposite films is given by

$$J_{sr}(s) = G_R(s)I_R(s) + G_Z(s)I_Z(s) \tag{1}$$

(11) (a) Ruland, W. *J. Appl. Crystallogr.* **1971**, *4*, 70−73. (b) Siemann, U.; Ruland, W. *Colloid Polym. Sci.* **1982**, *260*, 999−1010.

(12) Jeppesen, C.; Kremer, K. *Europhys. Lett.* **1996**, *34*, 563.

(13) Smarsly, B.; Kuang, D.; Antonietti, M. *Colloid Polym. Sci.* **2004**, *282*, 892−900.

(14) Larson, R. G.; Scriven, L. E.; Davis, H. T. *J. Chem. Phys.* **1985**, *83*, 2411.

(15) (a) Larson, R. G. *J. Chem. Phys.* **1988**, *89*, 1642. (b) Larson, R. G. *J. Chem. Phys.* **1989**, *91*, 2479. (c) Larson, R. G. *J. Chem. Phys.* **1992**, *96*, 7904.

(16) (a) Smarsly, B.; Polarz, S.; Antonietti, M. *J. Phys. Chem. B* **2001**, *105*, 10473−10483. (b) Smarsly, B.; Goltner, C.; Antonietti, M.; Ruland, W.; Hoinkis, E. *J. Phys. Chem. B* **2001**, *105*, 831−840. (c) De Paul, S. M.; Zwanziger, J. W.; Ulrich, R.; Wiesner, U.; Spiess, H. W. *J. Am. Chem. Soc.* **1999**, *121*, 5727.

where

$$I_R(s) = \langle |\Phi_R|^2 \rangle(s) - |\langle \Phi_R \rangle|^2(s)$$

$$I_Z(s) = |\langle \Phi_R \rangle|^2(s) \left[\frac{1}{N} |Z_{h0}|^2(s) - 1 \right]$$

$$G_Z(s) = \frac{\pi}{4asB_{ax}}$$

$$G_R(s) = \frac{\pi}{2} + \ln(y_{max}/\sin(B_{ax}/2)) - \frac{1}{2}\ln(s^2 + y_{max}^2)$$

B_{ax} represents the integral width of the axial orientation distribution g_{ax} and is a measure of the degree of orientation of the mesostructure.[7] y_{max} is defined as the half of the width of the slit function $W(y)$. To the best of our knowledge, this approach represents the first theoretical concept to determine the degree of preferred orientation (measured as B_{ax}) in combination with a quantitative determination of pore sizes in 2D hexagonal arrays of thin films.

2. Final Expression for Fitting of SAXS Data. To take into account a finite width of the interface between silica and the micelles, a suitable approach is given by multiplying eq 1 by the function $H_z^2(s) = \exp(-2\pi d_z^2 s^2)$,[11] where d_z is the thickness of the interface boundary. In addition, the SRSAXS data have to be corrected by an absorption correction; we use $A(\theta) \propto 1 - \exp[-2\mu t/\sin\theta]$.[7,8] The linear absorption coefficient μ was approximated to be ~ 40 cm^{-1}.[8] The final function to fit the SRSAXS data is therefore given by

$$J_{fit} = kAH_z^2[G_R I_R + G_Z I_Z + I_B] \qquad (2)$$

where k is a scaling factor and I_B represents the background scattering due the density fluctuations, which was supposed to be constant in the present case.[11] Possible scattering from the interference boundaries substrate–film and film–air was neglected in the analyses. A quantitative investigation of this weak contribution in mesostructured films will be the subject of a separate study. Hence, the fitting parameters are $\bar{R}$, σ_R, $\bar{a}$, σ_a, $\bar{N}$, σ_N, B_{ax}, d_z, k, and I_B.

Results and Discussion

1. TEM Analysis. The TEM analysis confirmed a highly ordered mesostructure for all samples under study. As a representative example, Figure 3 shows two TEM images obtained for sample 2, revealing an extended domain of a 2D hexagonal pattern, with the lattice parameter ($\sim 6-7$ nm) being in agreement with those obtained from GISAXS and SRSAXS (see below). The layer structure corresponds to the side view of the cylinders. It is noteworthy that the cylinder length is on the order of several hundred nanometers/microns, which substantially exceeds the cylinder radius. Thus, the TEM micrographs support the interpretation of the GISAXS data in terms of a 2D hexagonal mesostructure of long cylinders with a high degree of order.

2. GISAXS. Grazing incidence SAXS (GISAXS) experiments were carried out to verify the presence of a highly oriented 2D hexagonal mesostructure. The 2D GISAXS of sample 2 (Figure 4A) shows diffraction spots that can be attributed to a 2D hexagonal lattice of cylinders with the cylinders being oriented parallel to the substrate. From the GISAXS pattern itself, we obtain an apparent lattice parameter $a \approx 6.2-6.4$ nm, which is in semiquantitative
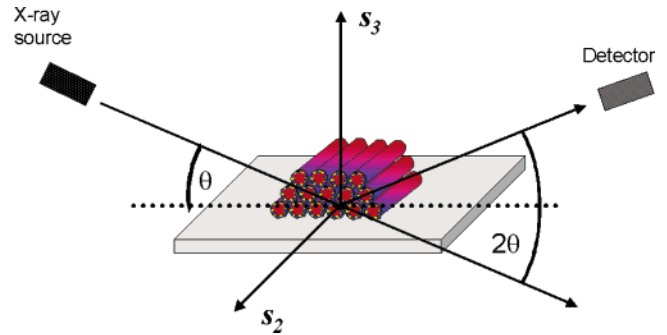

Figure 2. Schematics of SAXS in symmetric reflection, applied to a system of cylindrical micelles arranged in a 2D hexagonal lattice, oriented parallel to the substrate.
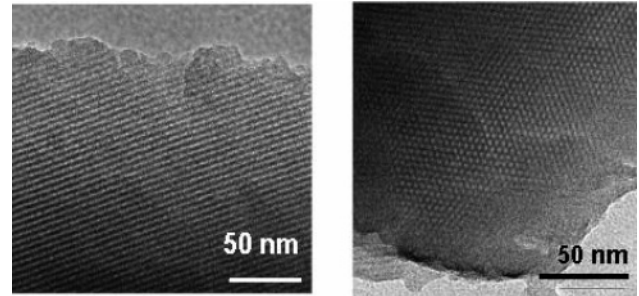

Figure 3. Transmission electron micrograph images of sample 2, showing the cylinders parallel (left) and perpendicular (right) to the cylinder axis.
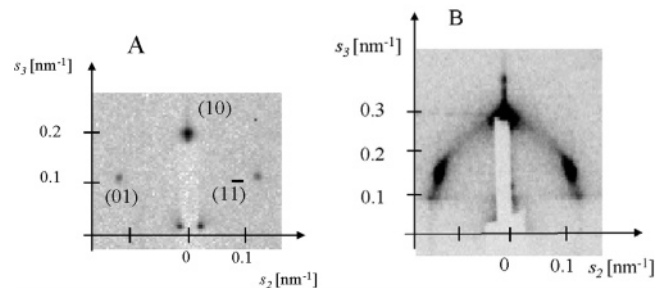

Figure 4. 2D GISAXS patterns of sample 1: (A) uncalcined; (B) after calcination at 450 °C for 3 h.

agreement with the TEM results and SRSAXS experiments. Also, the small spot size of the reflections indicates a high degree of regularity of the 2D hexagonal mesostructure. It is also seen that the mesostructure is slightly contracted in the s_3 (z) direction, perpendicular to the substrate, which is well-known for dip-coated thin mesostructured films. Similar results were obtained for all of the films. The GISAXS experiment was repeated on the same film (not shown) 1 year after its original preparation, showing still a highly ordered 2D mesostructure together with a slight contraction of the whole mesostructure as indicated by a decrease to $a \approx 5.9-6.1$ nm (in the direction of s_3), that is, by $\sim 10\%$. In conclusion, it can be safely stated that the films under investigation indeed possess a highly organized, oriented, and stable 2D hexagonal mesostructure.

3. Analysis of SAXS Data in Symmetric Reflection of Self-Assembled Nanocomposite Silica–Surfactant Mesostructured Films. To illustrate the influence of the width of the distribution of radii on the SRSAXS patterns, Figure 5 shows a series of simulations of such curves under variation of σ_R, keeping the other parameters constant. The parameters were chosen similar to those obtained for the present materials. It is seen that the interference minima become broader with increasing
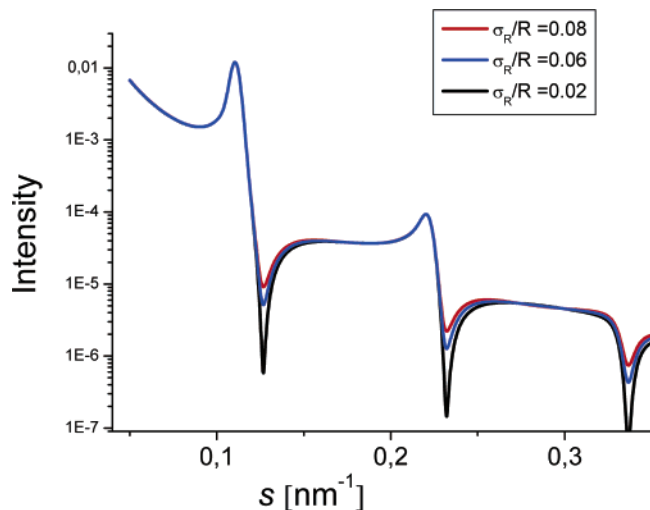
Figure 5. Simulation of SAXS data in symmetric reflection based on eq 2, as a function of different values for σ_R/R, with the other parameters kept constant. The parameters used for the simulations are $\bar{R} = 30.0$ Å, $\bar{a} = 65.0$ Å, $\sigma_a = 1.5$ Å, $d_z = 5$ Å, $I_B = 0$, $B_{ax} = 0.03°$, $\bar{N} = 15$, $y_{max} = 0.2$ nm^{-1}, $t = 400$ nm, and $\mu = 40$ cm^{-1}.
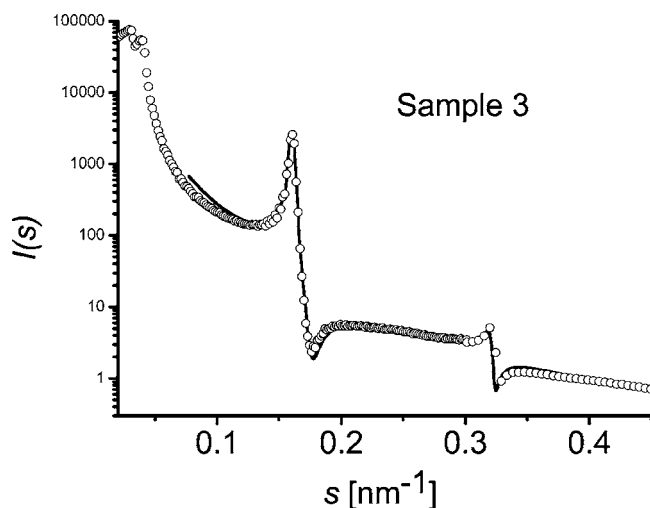
Figure 6. SAXS data in symmetric reflection (hollow circles) and fitting (solid curve) for sample 3 (Brij 58, $c/c_0 = 1.1$).

$\sigma_R/\bar{R}$. In conclusion, the simulation demonstrates that for small but finite values of σ_R the form factor minima should be observable by a suitable experimental setup.

The SRSAXS data were fitted using eq 2. To illustrate the high quality of the data fitting, Figure 6 shows as a representative example the scattering curve of sample 3 with a thickness of $t = 320$ nm as determined by spectroscopic ellipsometry (in ref 7, we had shown sample 1). It is seen that the data are well fitted over almost the whole range of accessible scattering vectors s, in particular the profiles of the maxima and minima. No Kiessig fringes are observable, which may be a consequence of the relatively large thickness and a certain degree of thickness inhomogeneity. It has to be pointed out that a "two-phase" model is sufficient to fit the SRSAXS data of all samples, with the surfactants forming the cylinder phase and the silica forming the surrounding matrix. As a main benefit of the reasonable fitting, various structural parameters are obtained with good accuracy (see Table 1). The precision in the determination of $\bar{R}$ turned out to be better than 1 Å, which is related to the well-defined position of the form factor minimum. In addition, a small but non-negligible size polydispersity is present with $\sigma_R/\bar{R} = 0.012$.
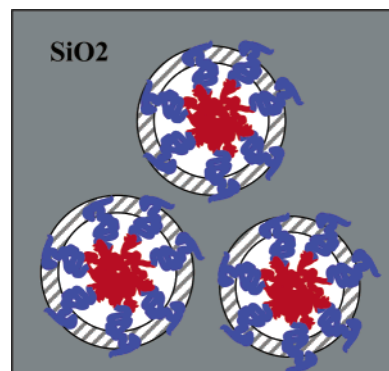

Figure 7. Illustration of the distribution of the surfactant within the silica−hybrid mesostructured film. The tails of the surfactant are colored in red, and the PEO headgroup chains, in blue. The transition zone for the present materials consisting of interdigitated silica−PEO is of measurable thickness (stripes).

Hence, EISA has to be regarded as a unique technique for fabricating mesostructures with comparably low polydispersities in the size of the constituting objects. Interestingly, a substantial value for d_z is observed ($d_z = 0.4-0.5$ nm), which is reasonable for Brij surfactants, assuming that PEO interacts with silica and forms a PEO-enriched silica "corona" of width d_z.[10] The calculation of the wall thickness by $w = \bar{a} - 2\bar{R}$ leads to an unrealistically small value of $w \approx 5$ Å. On the basis of the aforementioned interpretation of d_z,[10] a physically more reasonable definition of the wall thickness is given by

$$w \approx \bar{a} - 2\bar{R} + d_z \qquad (3)$$

From this definition, we obtain $w = 8.7$ Å for sample 1 and similar values for the other samples. (Accordingly, a more realistic value for the cylinder radius would be $\bar{R}_{corr} = \bar{R} - 0.5d_z$.) Regardless of the interpretation of d_z, the values $\bar{R}_{corr}$ and $\bar{a}$ indicate a dense packing of the cylinders with quite thin walls, which is in agreement with previously reported 2D hexagonal mesostructured films.[6] The relative sizes of the micelle, the "transition" zone, and the wall thickness are illustrated in Figure 7. The parameter σ_a, introduced to describe lattice distortions, has a small value, further confirming the high degree of mesostructural regularity. The parameter B_{ax}, describing the degree of preferred orientation, could be only determined for samples 1−3 and was in the range of 0.03°, indicating a highly oriented mesostructure in all cases.

4. Influence of the Surfactant Concentration. The high precision of the SRSAXS analysis therefore allows depicting fine structural changes upon changing the composition, in particular the surfactant concentration. The amount of surfactant was slightly changed such that a highly ordered 2D hexagonal phase was still formed, with the concentration of sample 2 being set as reference c_0. A wormlike mesostructure was observed if the concentration was varied too much. In all three cases, the SRSAXS curves, showing pronounced diffraction maxima and minima, could be reasonably fit over a large region of scattering vectors (Figure 8). The patterns indicate a shift of the maxima to smaller s with increasing concentration. A similar trend was observed for the interference minima. For samples 4−6 (Brij 56−silica), the parameters $\bar{R}$ and $\bar{a}$ changed accordingly (Figure 9). In summary, the analyses reveal an increase in both $\bar{a}$ and $\bar{R}$ of ∼6−8% from $c/c_0 = 0.9$ to $c/c_0 = 1.1$. Interestingly, the average wall thickness did not show a trend in this series and seemed to fluctuate statistically. It is therefore concluded that the increase in $\bar{a}$ is exclusively a consequence of an
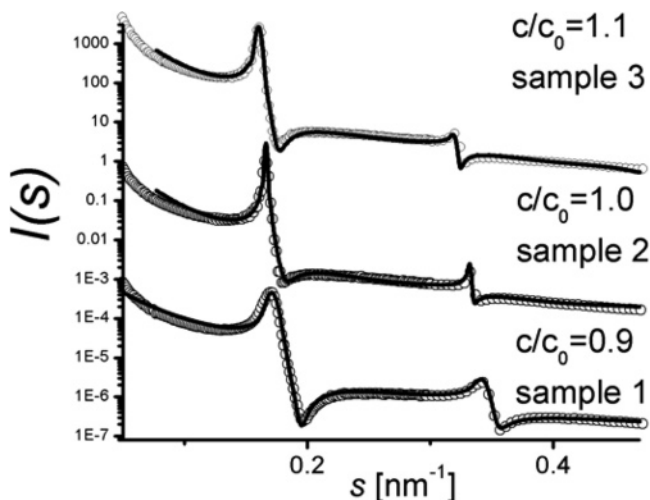
Figure 8. SRSAXS data (hollow circles) and fitting curves (solid lines) for Brij 58-templated silica films with 2D hexagonal mesostructures, using different surfactant concentrations c/c_0.
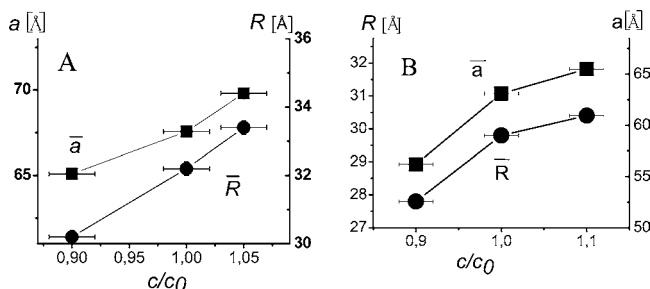

Figure 9. Dependence of the average micellar radius $\bar{R}$ (circles) and the lattice parameter $\bar{a}$ (squares) on the surfactant concentration for (A) Brij 58- and (B) Brij 56-templated silica films. The points are connected for better visualization.

increase in $\bar{R}$. Furthermore, it is noteworthy that the evaluation approach is able to depict such small changes on the angstrom scale. All of the samples show non-negligible values for σ_R and σ_a. These materials represent a rare example in which the scattering minima from the form factor are observable in solid mesostructured materials.

A comparison of the structural parameters of the two surfactants clearly demonstrates that for identical concentrations (i.e., an identical surfactant/SiO$_2$ ratio) the micelles are larger in the Brij 58-templated film compared to the Brij 56 system. This difference in $\bar{R}$ and $\bar{a}$ is reasonable taking into account that the hydrophobic tail of Brij 58 is substantially larger than that of Brij 56 ("C16" versus "C10"), thus leading to larger micellar cores.

For monodisperse cylinders, the position s_1 of the first minimum is related to the cylinder radius R_1. It should be noted that the determination of the radius from the position of the minima is not exact due to the finite size distribution. For monodisperse cylinders, the position s_1 of the minimum is related to the cylinder radius R_1 by

$$s_1 = \frac{0.610}{R_1} \tag{4}$$

The micelle radii determined by this relationship systematically exceed those obtained from the fitting despite the small polydispersity (Table 1). In conclusion, the increase in the cylinder radius is observed for two different surfactants and can be related to a generalized mechanism. For poly(ethylene oxide) (PEO)-containing block copolymer surfactants, it was previously demonstrated that the
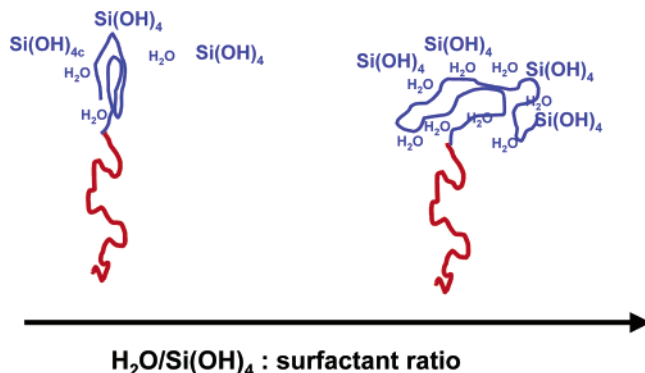

H$_2$O/Si(OH)$_4$: surfactant ratio

Figure 10. Illustration of the changes in the headgroup size and packing parameter upon increasing the surfactant/water ratio for nonionic Brij surfactants containing poly(ethylene oxide) headgroups (in blue color).

behavior of PEO in the templating/sol−gel procedure is strongly dependent on the state of hydration of the hydrophilic PEO. The strong interaction of hydrated PEO chains with siliceous species gives rise to micropores found in mesoporous silicas.[10] An increase in the Brij concentration in relation to the silica−water system would reduce the amount of water being able to swell the PEO block, thus reducing the headgroup size of the polymers and leading to a larger aggregation number and, thus, to a larger micelle radius (Figure 10). Indeed, a straightforward calculation reveals a molar ratio between water and Brij 58 PEO units of 1:2.2 (for sample 3), which is on the borderline of an optimum solvation of EO groups by water.[12] It is well-known that PEO chains collapse if the water content decreases below a critical value, thus leading to changes in the headgroup area in PEO-containing surfactants. This interpretation is supported by a recent study on low-molecular-weight ionic surfactants, addressing the influence of the surfactant concentration on the finally obtained cylindrical mesopores.[13] Contrary to the results of the present study, in that case, almost no change in the mesopore size was observed as a function of the surfactant concentration, while the wall thickness changed significantly.

Monte Carlo Simulations of the Self-Assembly of Cylinders

To investigate the nature of the changes in micellar size upon surfactant concentration, a lattice Monte Carlo (MC) simulation for a mixture of water and surfactant was carried out. The lattice model employs a simple cubic (SC) lattice with a coarse grained (lattice gas) representation of the fluid, whereby each lattice site can be occupied by at most one species. In this study, water is represented as a single bead occupying a single lattice site. The surfactant is represented through a linear chain of four hydrophobic beads (T4), representing the tail, and a branched hydrophilic headgroup with three beads (H3) (see Figure 11). This modeling approach follows the work of Larson.[14,15] For the interactions between the involved molecules, we restrict ourselves only to nearest-neighbor interaction. The water−water interaction was set to 1 and is identical to the water−head interaction. The unfavorable interaction of the hydrophobic tail with water and the hydrophilic head was set to 0. The first step in the calculation was to find a composition of surfactant (H3T4) and water forming a hexagonal structure. This structure acted as the starting point for finding hexagonal structures with less amount of surfactant, which was done by replacing the surfactant chains in the starting structure
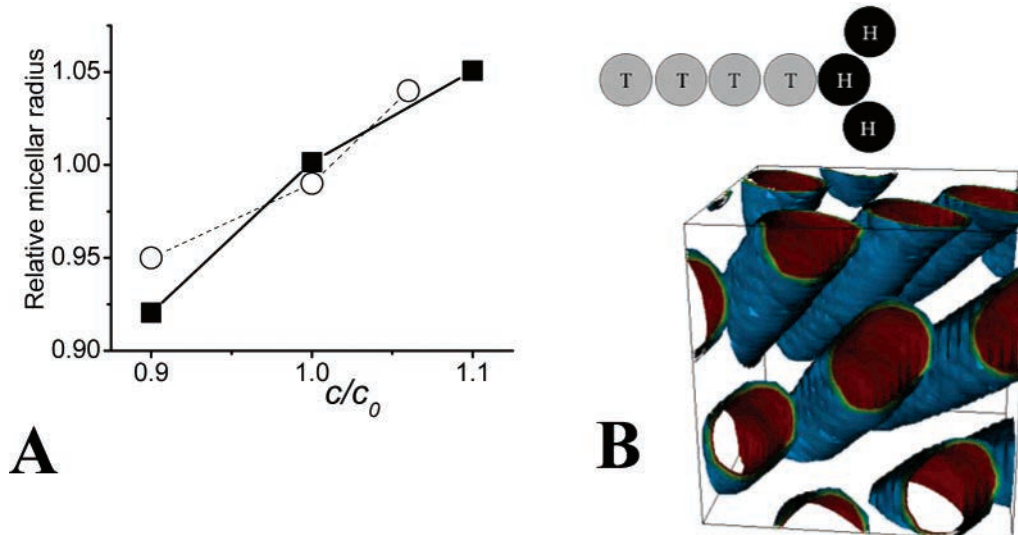
Figure 11. Monte Carlo simulation of the influence of surfactant concentration on 2D hexagonal micellar mesophases for a H3T4 surfactant: (A) changes in the micelle radius, as a function of the surfactant concentration (simulation), compared to the experimental results (Brij 58−silica); (B) sketch of the H3T4 model surfactant (top) and illustration of the simulated cylindrical mesophases (cross section, bottom).

by water. The following energy minimizations gave hexagonal structures as a result. The estimation of the radius was done by using Python (www.python.org, 2004) and the Visualization Toolkit VTK (www.kitware.com, 2004). In this simulation, the surfactant concentrations were chosen similar to our experiments ($0.9 < c/c_0 < 1.1$). It is seen (Figure 11) that the radius of the cylindrical domains increases monotonically with increasing surfactant concentration, which is in good agreement with our experimental findings. Although these simulations cannot be regarded as quantitative on an absolute scale, the relative increase in R between $c/c_0 = 0.9$ and $c/c_0 = 1.1$ is comparable to that observed in our experiments. In conclusion, both the concept of the packing parameter and MC simulations are in good agreement with the experimental data from two nonionic surfactants. The MC simulations suggest that the influence of surfactant concentration on the cylinder radius is due to the bulky character of the PEO headgroup.

Templating Behavior of PEO Homopolymers

The aforementioned results indicate that under the present conditions the majority of the PEO chains retract from the siliceous pore walls, form a separate layer on the hydrophobic core, and consequently do not lead to microporosity in the walls, as reported for similar systems.[16] Furthermore, it was discussed that the hydration of PEO in the templating process determines the generation of micropores in the pore walls.[16] To further elucidate the porosity induced by PEO in block copolymer templating, we prepared a series of porous silicas, obtained from TEOS as the silica source and PEO as the molecular template under variation of the PEO/water ratio, but while maintaining identical conditions with respect to the acid content, temperature, and so forth (see the Experimental Section). Hence, the composition was chosen similar to the thin films obtained from the Brij templates. The porosity of these PEO-templated silicas was studied by SAXS and nitrogen sorption. Figure 12 shows the porosity of these silicas, determined from the adsorption branch of nitrogen sorption according to the Barrett−Joyner− Halenda (BJH) approach, as a function of the molar PEO/ water ratio. Interestingly, the increase in the pore size is not linear but raises abruptly at $m(\text{PEO})/m(\text{water}) \approx 2$.
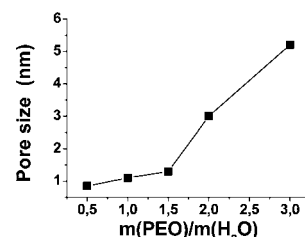

Figure 12. Dependence of the pore size of porous silica prepared with PEO homopolymer as the template, as a function of the molar PEO/water ratio.

It has to be pointed out that these values cannot be regarded as absolute numbers but are just considered to show a qualitative trend. The size change in the PEO-templated pores can be attributed to the decreasing degree of hydration while increasing the polymer content relative to water, thus inducing a conformational change. Consequently, at higher $m(\text{PEO})/m(\text{water})$ ratios, PEO is not templated as single chains but as agglomerates of several chains. In the case of amphiphilic templates such as Brij polymers, at high polymer/water ratios, the PEO forms a separate layer on the hydrophobic core and does not penetrate the silica walls. In the present case of PEO-containing surfactants, the PEO/water ratio (2.2:1) therefore has a value which corresponds to a low solubilization of PEO, which contributes to the mesoporosity rather than micropores.

Investigation of Mesoporous Films

Since the algorithm presented above turned out to provide reliable data for micellar parameters, it is self-evident to apply it to mesoporous films. Thereby, it was attempted to test the applicability of the theoretical SRSAXS approach also for porous films obtained from calcining samples 1−3. Figure 4B shows the GISAXS pattern of a film corresponding to sample 2 after calcination at 450 °C for 3 h, which leads to a complete decomposition of Brij surfactants. The GISAXS patterns clearly reveal a distortion of the 2D hexagonal structure upon calcination, and the mesostructure is shrunken preferentially perpendicular to the substrate, which was already reported recently.[6] Interestingly, B_{ax} increases
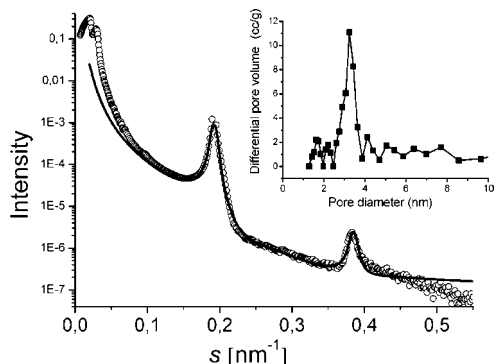
Figure 13. SAXS data in symmetric reflection (hollow circles) and fitting (solid line) of sample 2 calcined at 450 °C. The inset shows the corresponding pore size distribution, obtained from the desorption branch of a nitrogen sorption isotherm.

only slightly from $B_{ax} = 0.03°$ to $B_{ax} = 0.1°$; thus, a moderate decrease in the degree of preferred orientation occurs upon calcination. GISAXS reveals that the lattice parameter parallel to the substrate is $\sim$8–10% larger than that perpendicular (a_{perp}) to the surface, as determined from SRSAXS. Hence, the porous film mesostructure represents a distorted but still highly ordered 2D lattice. The SRSAXS data (Figure 13) confirm a substantial decrease in the mesostructural dimension as is seen in the shift of the first-order interference maximum. The maxima at small $s \approx 0.02$ nm^{-1} originate from the total reflection of the primary beam. From the fitting procedure, we obtain $\bar{R}$ = 14.0 Å (σ_R = 0.9 Å) and $\bar{a}$ = 37.8 Å (σ_a = 1.0 Å), with both values being much smaller than those for the uncalcined sample. σ_R is significantly larger than that for the uncalcined material, probably due to distortions and stress during calcination. Within the margin of experimental error, d_z is slightly larger than those for the uncalcined material and reasonable in light of the inherent small roughness of amorphous silica. However, the values for d_z have a significant error because the data are not fitted satisfactorily at larger s. For the calcined versions of the samples, a similar trend was observed with respect to the dependence of the pore size on the surfactant concentration. The wall thickness defined as $w = \bar{a} - 2\bar{R} + d_z$ leads to values of the order of approximately $w = 1.5$ nm, which seems reasonable with respect to the mechanical stability, but exceeds the values for the hybrid materials. Interestingly, already the wall thickness defined as $w = \bar{a} - 2\bar{R}$ is significantly larger than that for the hybrid material, which could be due to a matrix compaction and rearrangement due to the heat treatment, perpendicular to the substrate. Although the values for w involve a certain uncertainty, a trend is observed toward thinner walls from samples 1–3 and 4–6, going parallel with higher surfactant concentration. These differences in the wall thickness are reasonable in light of the increase in the pore size due to a higher surfactant/silica ratio.

The fit of the SRSAXS data is reasonable at up to $s = 0.4$ nm^{-1}, whereas it is not yet satisfactory at larger s, although the calcined materials represent a simpler system, just consisting of amorphous SiO$_2$ and voids. So far, we have no explanation for this systematic deviation. It is possible that the microporosity, generally observed in such materials, interferes with the SRSAXS evaluation in eq 2, which does not take into account micropores in the walls. Another possible reason could be the inhomogeneous deformation of the cylindrical pores normal to the substrate due to calcination.

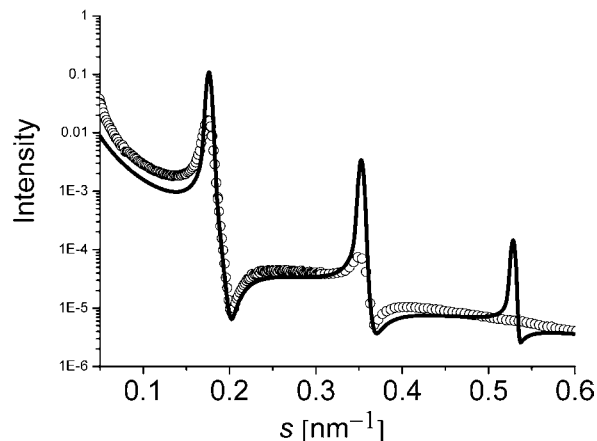Nitrogen sorption experiments were carried out on material scratched off from the mesoporous silica films to

Figure 14. Evaluation of the SRSAXS data (solid line) of sample 1 (hollow circles) assuming monodisperse cylinders, the absence of lattice imperfections, a uniform stacking number of $N = 60$ (corresponding to the film thickness), $d_z = 0$, and a perfect orientation of the arrays with respect to the substrate.

provide the pore radius by an independent technique. Figure 13 (inset) shows the BJH pore size distribution for sample 2, determined from the desorption branch, revealing an average pore size of $\sim$3.2 nm, which is in good semiquantitative agreement with the value evaluated from SRSAXS. However, the sorption analysis suffered from the low quantity of silica obtained from the films ($\sim$2 mg), thus imposing a substantial uncertainty on the absolute value of the pore size. Krypton sorption experiments are planned to perform a systematic comparison between the pore sizes obtained for SRSAXS and physisorption, allowing for a validity check of both techniques.

Conclusions/Discussion

In the present study, highly oriented mesostructured surfactant–silica nanocomposite thin films with a 2D hexagonal mesostructure of cylindrical micelles were prepared by EISA and studied by X-ray scattering in symmetric reflection, using two different nonionic Brij surfactants as model systems under variation of the surfactant/silica ratio. A recently developed procedure was developed to analyze the scattering data, and the approach could fit the data of all samples excellently over almost the entire range of accessible scattering data, thus allowing the determination of the micelle radius and the lattice parameter with a so far inaccessible accuracy of $\sim$1 Å. In addition, for the first time, it was possible to estimate the polydispersity of the micelles in thin films and the degree of lattice distortion of the 2D mesostructure. It is important to emphasize that the polydispersities in R and a have a significant effect on the scattering data, as well as d_z and the degree of preferred orientation B_{ax}.

The relevance of these parameters for a reasonable evaluation of the data is illustrated in Figure 14, showing the fitting of sample 1 using a model assuming monodisperse cylinders, the absence of lattice imperfections, a uniform stacking number of $N = 60$ (corresponding to the film thickness), $d_z = 0$, and a perfect orientation of the arrays with the respect to the substrate. Under these assumptions, the expression in eq 2 reduces to

$$J_{fit} = kA[I_z + I_B],$$

$$\text{where } \left[\frac{1}{N}|Z_{h0}|^2(s) - 1\right] = \left(\frac{\sin(\pi N d_{10} s)}{\sin(\pi d_{10} s)}\right)^2 \quad (5)$$

By these values, it is supposed that the interfacial

boundary is infinitely sharp and that the layers extend from the bottom to the top of the film. While the analytical curve would be superimposed by oscillations from the trigonometric term in the lattice factor, the expression has been smoothed by the convolution with a Gaussian distribution, to account for instrumental broadening. It is seen that this evaluation suffers from several aspects. First, the shape of the interference maxima cannot be fitted with acceptable accuracy, because the polydispersity in the cylinder radius and lattice distortions are not taken into account. A certain degree of lattice distortions has to be taken into account to describe the almost complete absence of the third interference maximum. It is worthy to note that the shape of the first minimum is adjusted with acceptable precision. Second, the overall slope (asymptotic behavior) is not described correctly by ignoring the finite width of the interface and the finite preferred orientation. The parameters obtained from fitting under these constraints are slightly different from that using the whole set of parameters; we obtain $R = 30.55$ Å and $a = 65.4$ Å. While the lattice parameter a is quite similar to $\bar{a}$, the radius R obtained in this way is significantly larger than $\bar{R}$. It is evident that this evaluation therefore omits a significant amount of information (polydispersity of the cylinders, lattice imperfections, degree of preferred orientation, and finite width of the phase boundaries), which can be obtained from the more extended analysis. However, it should be pointed out that the essential parameters R and a can be obtained with not too bad of an accuracy neglecting the other parameters, and therefore, a semiquantitative analysis could also be performed using eq 5.

As a main result, this study therefore demonstrates the validity of the approach introduced in ref 6 for such materials in general and its idea that X-ray scattering of thin mesostructured films, performed in symmetric reflection, provides an invaluable analytical tool. While in this previous study the self-assembled silica films were prepared from ionic surfactants, the present study proves that this general approach also applies excellently for other surfactant-templated films, and can be extended to a wide variety of thin mesostructured films. Our study shows that the introduction of more subtle structural parameters allows for a more precise evaluation of the scattering data. Future work will be devoted to a more general comparison of the present approach and analyses in terms of X-ray reflectivity approaches.[17]

On the basis of this high precision, our approach clearly revealed an increase in micellar sizes as a function of the surfactant concentration in the initial solution (surfactant/SiO_2 ratio), which could be attributed to the special templating behavior of poly(ethylene oxide) (PEO)-containing surfactant templates. Our study supports recent findings that the water content can play a crucial role in the self-assembly of thin mesostructured films, both silica[2h] and metal oxide films.[2i] Preliminary SAXS results and a recent study indicate that ionic surfactants do not show a comparable trend in the micellar size as a function of the surfactant/ratio.[13] This different behavior is probably due to the different affinity of ionic headgroups toward water, and also in the present case, the water/PEO ratio was relatively small. Since PEO chains are quite sensitive to the amount of water available in EISA, this sensitivity will aggravate a precise control of the mesopore radius in thin films. Furthermore, our results also provide further insights into the spatial distribution of the PEO chains in the self-assembly and sol−gel process. The SRSAXS analysis indicates that the silica walls consist of a pure SiO_2 phase of ~0.5 nm and a PEO containing transition zone in the vicinity of the surfactant cylinders of ~0.4−0.5 nm, thus being in good agreement with a recent study proposing a corona of micropore-containing silica around mesopores of SBA-15.[16c] Our analysis suggested that for the present formula for nonionic surfactants only a certain fraction of the PEO is intimately mixed with silica, while the majority probably retracts from the silica matrix.

(17) Gibaud, A. Specular reflectivity from smooth and rough surfaces. In *X-ray and Neutron Reflectivity: Principle and Applications*; Daillant, J., Gibaud, A.; Springer: Paris, 1999; pp 87−115.